

Supporting Information for “Coarsening dynamics of 2D subaqueous dunes”

P. A. Jarvis^{1,2,3}, K. A. Bacik^{1,4}, C. Narteau⁵ and N. M. Vriend^{6,1,7}

¹Department of Applied Mathematics and Theoretical Physics, University of Cambridge, Cambridge, UK.

²Department of Earth Sciences, University of Geneva, Switzerland.

³GNS Science, Wairakei Research Centre, New Zealand

⁴Centre for Networks and Collective Behaviour, Department of Mathematical Sciences, University of Bath, Bath, UK

⁵Institut de Physique du Globe de Paris, Sorbonne Paris Cité, Université Paris Diderot, Paris, France.

⁶BP Institute, University of Cambridge, Cambridge, UK.

⁷Department of Earth Sciences, University of Cambridge, Cambridge, UK.

Contents of this file

1. Text S1 to S2
2. Figures S1 to S5

Additional Supporting Information (Files uploaded separately)

1. Caption for large Table S1

Text S1.

In the OpenFOAM simulations, the initial velocity in the flume is zero everywhere, apart from the basal and side walls which are set to a velocity U . To enable better convergence of the numerical solution, a Reynolds-Averaged Simulation (RAS) (which

solves the Reynolds-Averaged Navier Stokes equations) is first performed computing 20 s of simulation time, which is observed to be long enough for the average horizontal flow profile to converge. The state of the system at this time is then taken as the initial state for the LES, which is again run for 20 s of simulation time. The horizontal flow profiles are then spatially- and temporally-averaged over the domain length and the last 10 s of simulation time, respectively. Both RAS and LES runs use the same mesh, which is fine enough to capture the detail of the flow profile in the lowermost part of the tank (20 cells in the lowermost 1 cm) whilst the timestep Δt was adjusted to respect the Courant-Friedrichs-Lewy (CFL) condition such that $|u|\Delta t/\Delta x \leq 0.1$ everywhere, where $|u|$ is the magnitude of the velocity field and Δx is the cell size (Courant et al, 1928).

Text S2.

Identification of individual peaks in the bed profile follows a method modified from Martin and Jerolmack (2013). First, measured profiles are filtered to remove spurious peaks, which can be caused by suspended sediment or marks on the walls of the flume, by imposing that bed slopes could be no greater than 0.5. We then define a baseline by calculating a moving average of each profile of window size p measurement points, and then subtracting this from the profile. Individual bedforms are then identified as being bounded by the zero-crossing points of this profile and the number of dunes n is counted at each time t_i . This differs from the routine of Martin and Jerolmack (2013) who used the global mean to define the baseline. However, we found this leads to errors, with smaller bedforms not being identified, and therefore refined this general algorithm. For a given experiment, the choice of p is chosen such that it minimises the parameter

$$\eta = \left(\sum_{i=l}^{N-1} n(t_i) \right)^{-1} \sum_{i=l}^{N-1} \max[n(t_{i+1}) - n(t_i), 0]. \quad (1)$$

Early profiles where individual bedforms are poorly defined have a significant effect on the selected value of η , and therefore we ignore the first 10 profiles and choose $l = 11$. Although this choice is somewhat arbitrary, the selected value of η was found to only weakly depend on choices of l from 6 to 30. The benefit of minimising η to choose p is that we ensure we capture as many small bedforms as possible, whilst not over-counting spurious peaks.

References

Martin, R. L., & Jerolmack, D. J. (2013). Origin of hysteresis in bed form response to unsteady flows. *Water Resour. Res.*, *49*, 1314–1333.

Table S1. List of experimental parameters: h = thickness of the erodible bed; H = depth of the water layer; ω_b = angular velocity of the rotating table; ω_t = angular velocity of the paddles; $\Omega = \omega_t - \omega_b$; $U = R\Omega$ where R is the radius of the channel; $r^* = |\omega_t/\omega_b|$; u_* is the estimated friction velocity at the bed surface; θ is the estimated Shields number; Δx is the spacing between measurement points, Re is the Reynolds number and a_z , b_z , a_λ and b_λ are the fitting parameters from equations 2 and 3 in the main manuscript, with Δa_z , Δb_z , Δa_λ and Δb_λ the associated uncertainties.

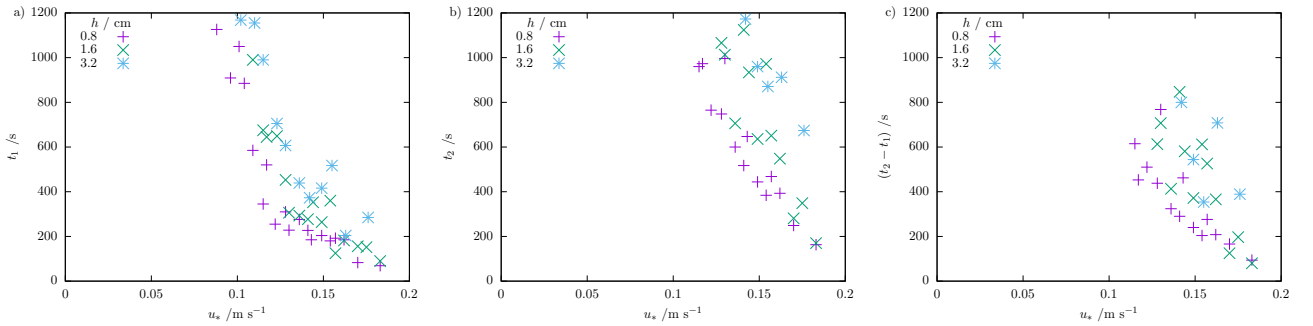


Figure S1. The dependence of a) t_1 , b) t_2 and c) $t_2 - t_1$ on u_* and h . It can be seen that both t_1 and t_2 , as well as the difference between them, rapidly decrease with increasing u_* . All three quantities also increase with h .

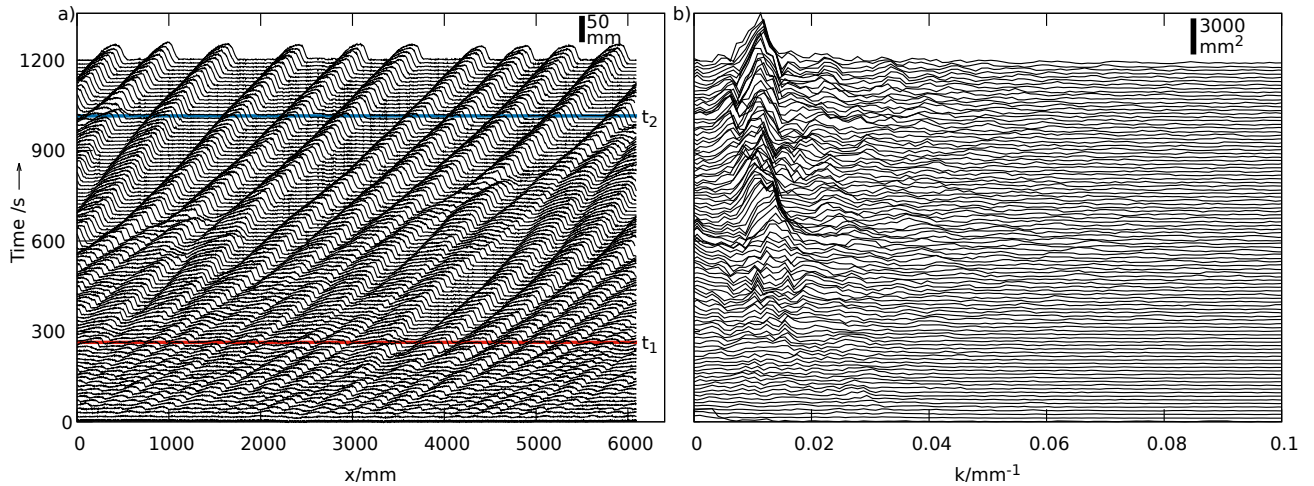


Figure S2. a) The bed profile $Z(x)$ and b) its Fourier transform $\tilde{z}(k)$ over 20 minutes for $H = 20$ cm, $h = 0.8$ cm and $U = 1.05$ m s $^{-1}$ (same experiment presented in Figure 2 of the main manuscript). Small perturbations form within 60 s whilst \tilde{z} remains flat showing no dominant wavelength. The profile coarsens as bedform interactions remove shorter wavelengths leading to the growth of a broad peak in \tilde{z} at $k \approx 0.01$ mm $^{-1}$. After ~ 300 s, flat sections in $Z(x)$ appear where the channel base has been exposed (t_1 , red line). Multiple patches of bare ground appear as the profile transitions from continuous to discrete dunes (t_2 , blue line), whilst the peak in \tilde{z} continuously narrows. Solid black bars indicate the vertical scale in both a) and b).

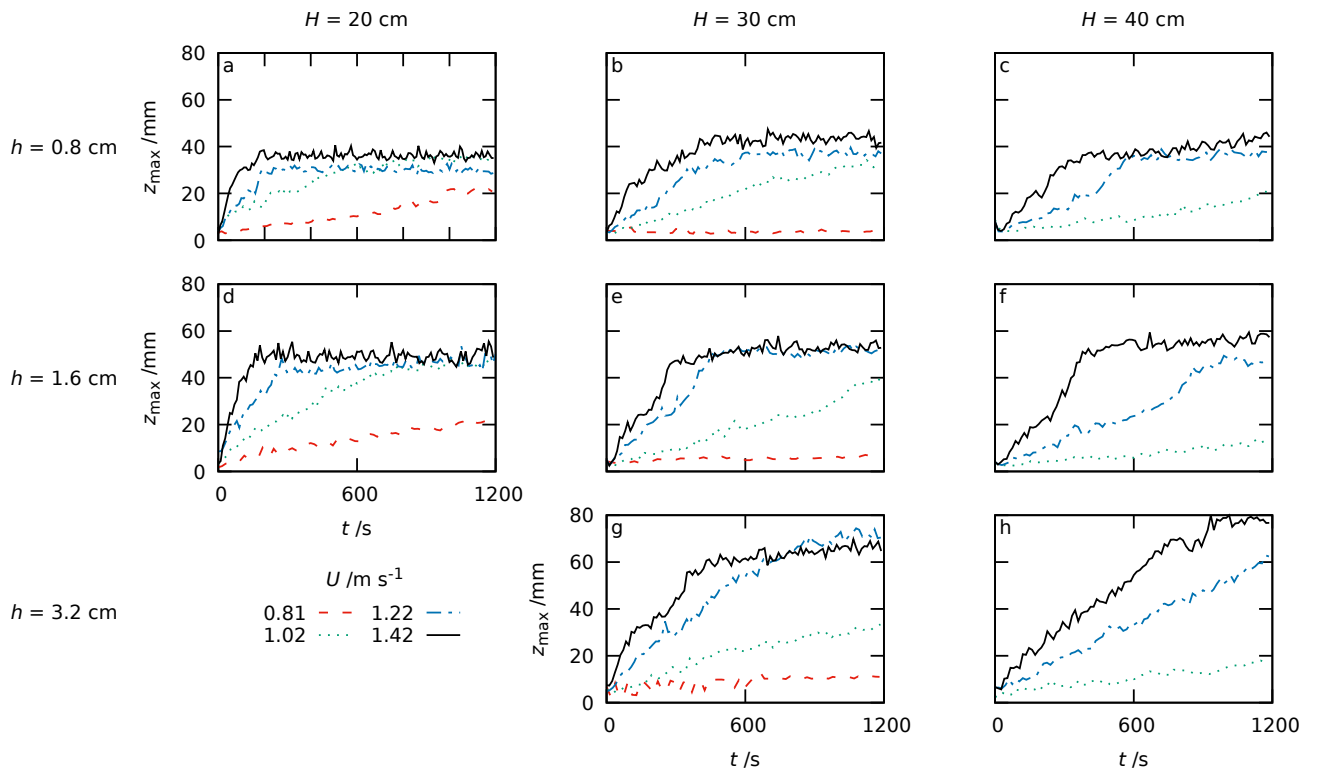


Figure S3. Temporal evolution of the ratio of the peak-to-peak bed amplitude z_{\max} for selected experiments.

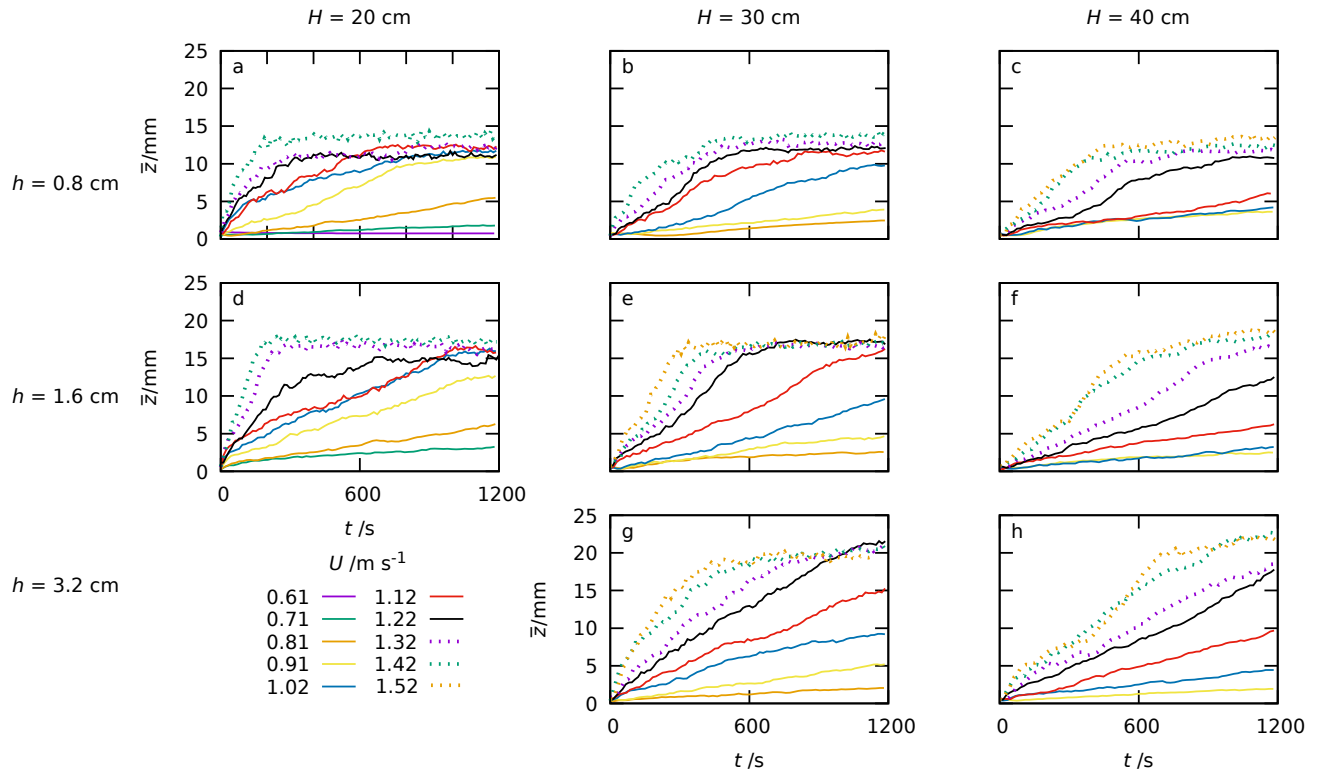


Figure S4. Temporal evolution of the root-mean squared bed amplitude \bar{z} for all experiments.

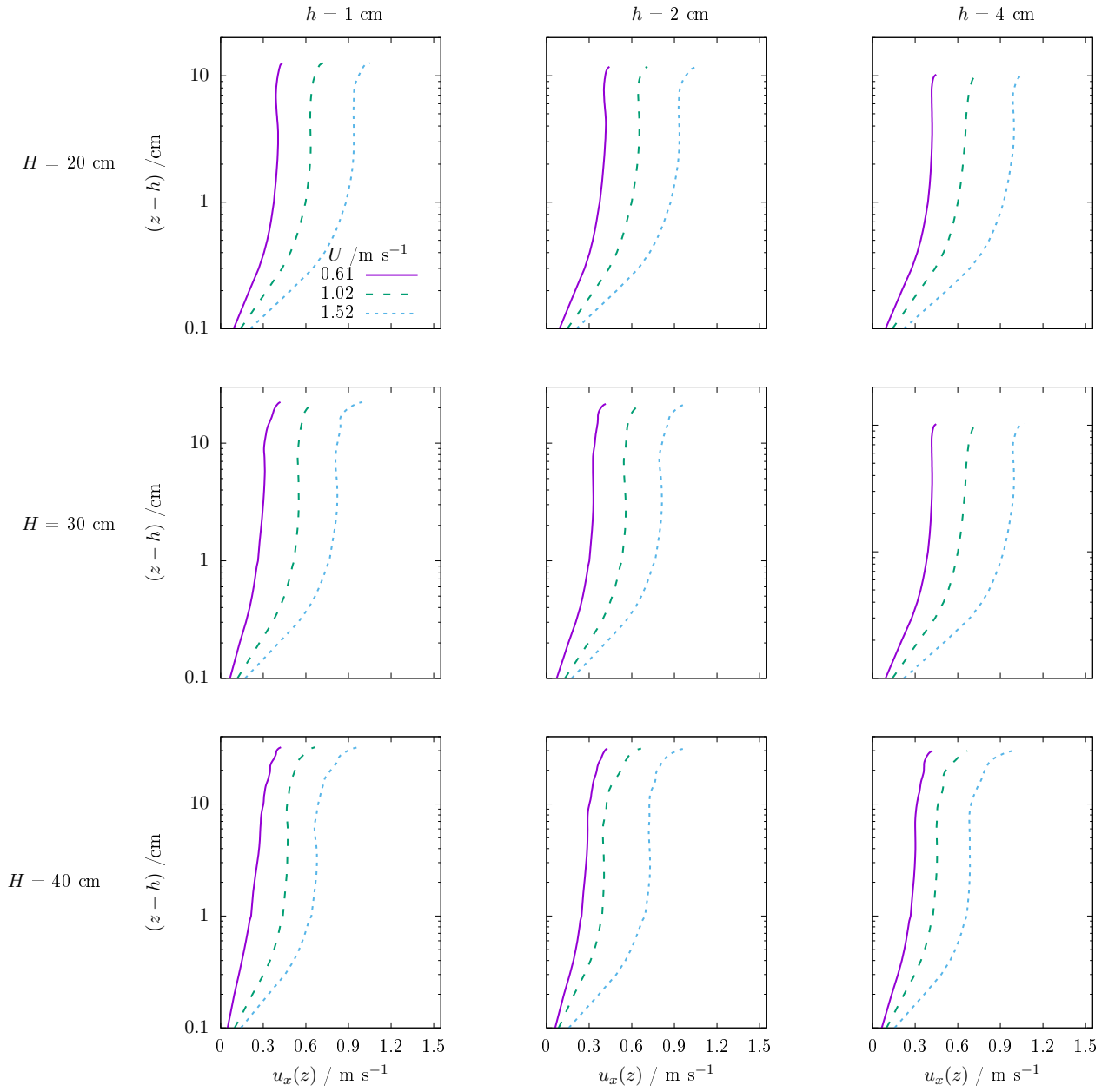


Figure S5. Simulated width-averaged velocity profiles $u(z)$ for a range of parameter values H , h and U that are utilised in the experiments.

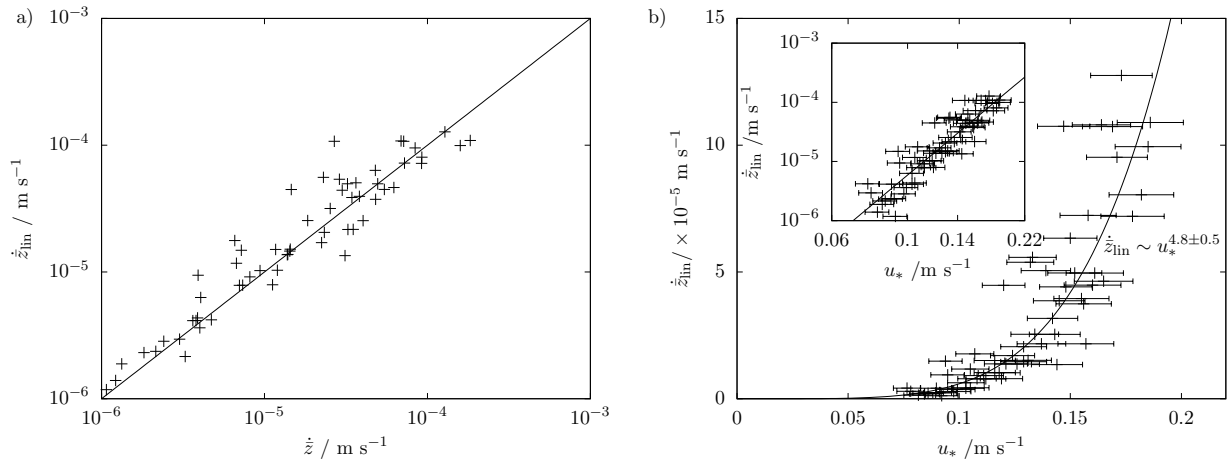


Figure S6. a) Comparison of different estimators of the initial dune growth rate. On the x axis is $\dot{z} = ab$, as determined from the fitting to the exponentially-saturated growth laws whilst on the y axis is \dot{z}_{lin} as determined from a linear fit to the initial part of the $\bar{z}(t)$ curves. b) Plot showing how \dot{z}_{lin} varies with u_* , as well as the fitted power law. The inset shows the same data but on logarithmic axes.

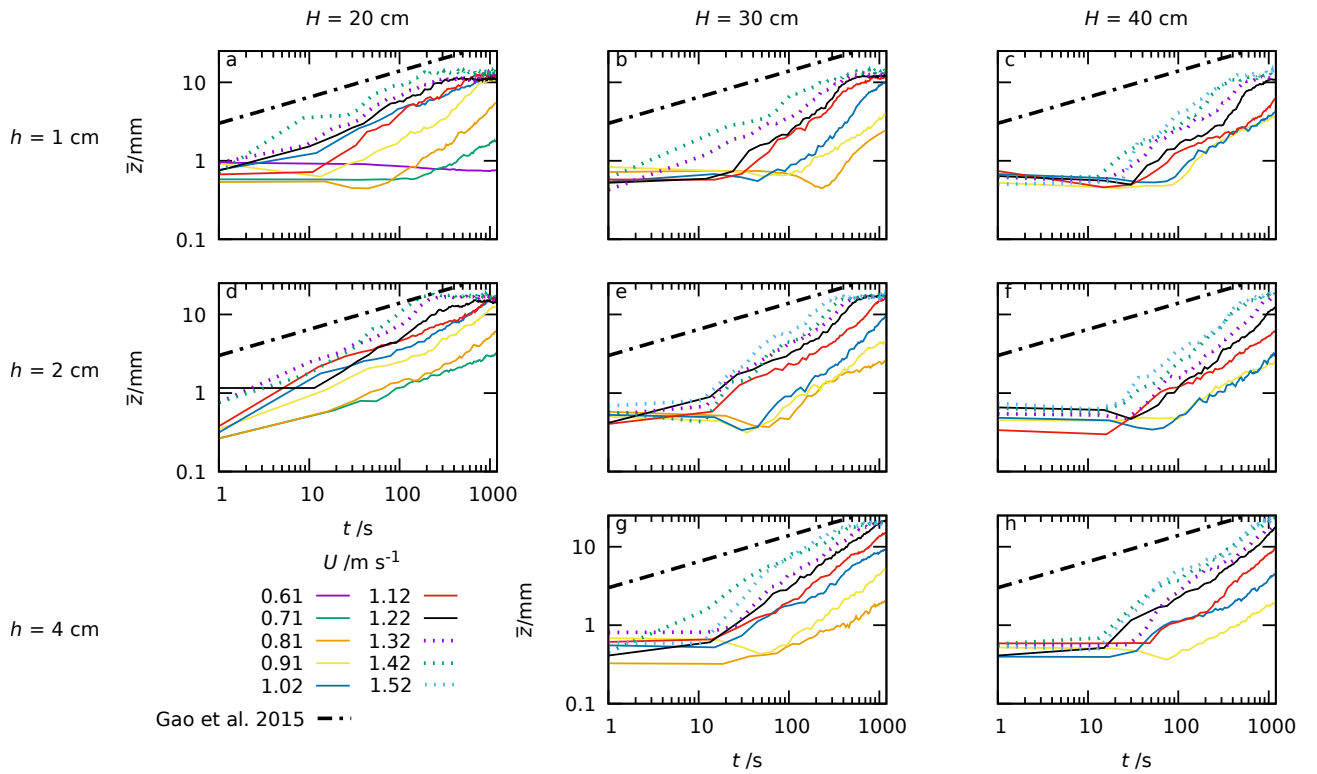


Figure S7. Root-mean squared amplitude \bar{z} of the sedimentary bed as a function of time t for different flow velocities U , initial bed thicknesses h , and flow depths H . The dashed-dotted black line shows the $t^{1/3}$ relation determined by Gao et al. (2015) for the coarsening of transverse bedforms in a cellular automaton model. We see that, after an initial period of no or slow growth, the bedforms in our experiments grow at a faster rate than the $t^{1/3}$ relationship. Fitting power laws to the data results in a wide range of exponents with no systematic dependence on U , H or h . Hence, we chose to use the exponentially-saturating fitting as presented in the main manuscript.